Research Article | Vol. 8, No. 7 | 1 Jul 2018 | OPTICAL MATERIALS EXPRESS 1902
Optical Materials EXPRESS

Processing and fabrication of micro-structures by multiphoton lithography in germanium-doped arsenic selenide

CASEY M. SCHWARZ,[1,2] CHRIS N. GRABILL,[1] GERALD D. RICHARDSON,[1] SHERYA LABH,[1] BENN GLEASON,[3,4] CLARA RIVERO-BALEINE,[5] KATHLEEN A. RICHARDSON,[4] ALEXEJ POGREBNYAKOV,[6] THERESA S. MAYER,[6] AND STEPHEN M. KUEBLER[1,4,*]

[1]*Chemistry Department, University of Central Florida, Orlando, FL 32816, USA*
[2]*Physics Department, Ursinus College, Collegeville, PA 19426, USA*
[3]*Clemson University, Clemson, SC 29634, USA*
[4]*CREOL, The College of Optics and Photonics, University of Central Florida, Orlando, FL 32816, USA*
[5]*Lockheed Martin, Orlando, FL 32819, USA*
[6]*Department of Electrical Engineering, Pennsylvania State University, University Park, PA 16802, USA*
**kuebler@ucf.edu*

Abstract: This work reports the processing and properties of a new chalcogenide glass film that can be photo-patterned by multiphoton lithography (MPL) with enhanced post-fabrication stability. Thermally evaporated germanium-doped arsenic selenide [$Ge_5(As_2Se_3)_{95}$] thin films were photo-patterned using the output of a mode-locked titanium:sapphire laser. The morphology, chemical structure, and optical properties of the material were studied before and after photo-patterning and compared for their long-term aging behavior and stability to previously investigated arsenic trisulfide (As_2S_3) films fabricated using similar MPL conditions. Relative to As_2S_3, thermally deposited $Ge_5(As_2Se_3)_{95}$ is found to offer higher photo-sensitivity and greater chemical stability after photo-patterning, as evidenced by lack of age-induced crystallization and reduced feature degradation over a four year aging period. These findings demonstrate the suitability of a new photo-patternable material for the creation of robust, long-lived functional infrared anti-reflective coatings and meta-optics.

OCIS codes: (140.0140) Lasers and laser optics; (310.0310) Thin films; (160.0160) Materials.

References and links

1. E. Hand, "Remote sensing. Carbon-mapping satellite will monitor plants' faint glow," Science **344**(6189), 1211–1212 (2014).
2. W. Zhang, Y. Shi, R. Hu, Y. Zeng, and M. Yan, "Application status and development trend of infrared imaging system," presented at International Symposium on Photoelectronic Detection and Imaging, Beijing, China, 25–27 Jun. 2013.
3. A. Ashcroft, L. Richardson, R. Ash, P. Thorne, D. Isgar, D. Jeckells, M. Stevens, T. Davey, and A. Malik, "A miniature ruggedized fast frame rate infra-red sensor module for hostile fire detection and industrial applications," presented at Infrared Technology and Applications XXXIX, Baltimore, Maryland, USA, 29 Apr. - 3 May 2013.
4. D. H. Cha, Y. Hwang, J.-H. Kim, and H.-J. Kim, "Fabrication and evaluation of chalcogenide glass molding lens for car night-vision system," presented at Integrated Optics: Physics and Simulations, Prague, Czech Republic, 15–18 Apr. 2013.
5. W. V. Moreshead, J. Novak, and A. Symmons, "An investigation of material properties for a selection of chalcogenide glasses for precision glass molding," Proc. SPIE **8541**, 854102 (2012).
6. A. Zelazny, R. Benson, J. Deegan, K. Walsh, D. W. Schmidt, and R. Howe, "Optical methods for the optimization of system SWaP-C using aspheric components and advanced optical polymers," presented at Infrared Technology and Applications XXXIX, Baltimore, Maryland, 29 Apr. - 3 May 2013.
7. G.-M. Ryu, G.-J. Lee, S.-W. Hyun, H.-Y. Sung, E. Chung, and G.-H. Kim, "A study on ultra precision machining technique for Al6061-T6 to fabricate space infrared optics," presented at Space Telescopes and Instrumentation 2014: Optical, Infrared, and Millimeter Wave, Montréal, Quebec, Canada, 22–27 Jun. 2014.
8. X. H. Zhang, Y. Guimond, and Y. Bellec, "Production of complex chalcogenide glass optics by molding for thermal imaging," J. Non-Cryst. Solids **326**, 519–523 (2003).

#330302 https://doi.org/10.1364/OME.8.001902
Journal © 2018 Received 26 Apr 2018; revised 29 May 2018; accepted 31 May 2018; published 13 Jun 2018

Optical Materials EXPRESS

9. H. Cha, H. J. Kim, H. S. Park, Y. Hwang, J. H. Kim, J. H. Hong, and K. S. Lee, "Effect of temperature on the molding of chalcogenide glass lenses for infrared imaging applications," Appl. Opt. **49**(9), 1607–1613 (2010).
10. H. Cha, H.-J. Kim, Y. Hwang, J. C. Jeong, and J.-H. Kim, "Fabrication of molded chalcogenide-glass lens for thermal imaging applications," Appl. Opt. **51**(23), 5649–5656 (2012).
11. J. L. Adam and X. Zhang, eds., *Chalcogenide Glasses: Preparation, Properties and Applications* (Woodhead Publishing Limited, Cambridge, 2014).
12. K. J. Ma, H. H. Chien, S. W. Huang, W. Y. Fu, and C. L. Chao, "Contactless molding of arrayed chalcogenide glass lenses," J. Non-Cryst. Solids **357**(11-13), 2484–2488 (2011).
13. B. Gleason, P. Wachtel, D. J. Musgraves, and K. Richardson, "Using design of experiments to improve precision molding of chalcogenides," Int. J. Experimental Design and Process Optimisation **3**, 263–275 (2013).
14. B. Gleason, "Designing Optical Properties in Infrared Glass," Ph.D. dissertation (Clemson University, Clemson, South Carolina, USA, 2015).
15. S. Wong, M. Deubel, F. Perez-Willard, S. John, G. A. Ozin, M. Wegener, and G. von Freymann, "Direct laser writing of three-dimensional photonic crystals with a complete photonic bandgap in chalcogenide glasses," Adv. Mater. **18**(3), 265–269 (2006).
16. C. M. Schwarz, S. Labh, J. E. Barker, R. J. Sapia, G. D. Richardson, C. Rivero-Baleine, K. A. Richardson, A. Pogrebnyakov, T. S. Mayer, and S. M. Kuebler, "Multi-photon lithography of 3D micro-structures in As_2S_3 and $Ge_5(As_2Se_3)_{95}$ chalcogenide glasses," Proc. SPIE **9759**, 975916 (2016).
17. C. M. Schwarz, H. E. Williams, C. N. Grabill, A. M. Lewis, S. M. Kuebler, B. Gleason, K. A. Richardson, A. Pogrebnyakov, T. S. Mayer, C. Drake, and C. Rivero-Baleine, "Processing and properties of arsenic trisulfide chalcogenide glasses for direct laser writing of 3D micro structures," Proc. SPIE **8974**, 89740P (2014).
18. C. M. Schwarz, C. N. Grabill, B. Gleason, S. Novak, A. M. Lewis, G. D. Richardson, C. Rivero-Baleine, K. Richardson, A. Pogrebnyakov, T. S. Mayer, and S. M. Kuebler, "Fabrication and characterization of micro-structures created by direct laser writing in multi-layered chalcogenide glass," Proc. SPIE **9374**, 937403 (2015).
19. S. M. Kuebler and M. Rumi, "Nonlinear optics–applications: three-dimensional microfabrication," in *Encyclopedia of Modern Optics*, R. D. Guenther, D. G. Steel, and L. Bayvel, eds. (Elsevier, Oxford, 2004).
20. P. J. Allen, B. R. Johnson, and B. J. Riley, "Photo-oxidation of thermally evaporated As_2S_3 thin films," J. Optoelectron. Adv. Mater. **7**(4), 1759–1764 (2005).
21. R. Bryce, H. T. Nguyen, P. Nakeeran, R. G. DeCorby, P. K. Dwivedi, C. J. Haugen, J. N. McMullin, and S. O. Kasap, "Direct UV patterning of waveguide devices in As_2Se_3 thin films," J. Vac. Sci. Technol. A **22**(3), 1044–1047 (2004).
22. J. K. Park, J. H. Lee, S. Y. Shin, J. H. Yi, W. H. Lee, B. J. Park, J. H. Choi, N. Y. Kim, and Y. G. Choi, "Compositional dependence of hardness of Ge-Sb-Se glass for molded lens applications," Arch. Metall. Mater. **60**(2), 1205–1208 (2015).
23. X. Su, R. Wang, B. Luther-Davies, and L. Wang, "The dependence of photosensitivity on composition for thin films of $Ge_xAs_ySe_{1-x-y}$ chalcogenide glasses," Appl. Phys., A Mater. Sci. Process. **113**(3), 575–581 (2013).
24. T. Wagner, S. O. Kasap, M. Vlcek, A. Sklenar, and A. Stroncki, "Modulated-temperature differential scanning calorimetry and Raman spectroscopy studies of As_xS_{100-x} glasses," J. Non-Cryst. Solids **2000**, 964–968 (1988).
25. D. J. Musgraves, P. Wachtel, S. Novak, J. Wilkinson, and K. Richardson, "Composition dependence of the viscosity and other physical properties in the arsenic selenide glass system," J. Appl. Phys. **110**(063503), 1–6 (2011).
26. A. Prasad, C.-J. Zha, R.-P. Wang, A. Smith, S. Madden, and B. Luther-Davies, "Properties of $Ge_xAs_ySe_{1-x-y}$ glasses for all-optical signal processing," Opt. Express **16**(4), 2804–2815 (2008).
27. R. Y. Golovchak, A. Kozdras, and O. Shpotyuk, "Physical ageing in glassy As–Se induced by above-bandgap photoexposure," Solid State Commun. **145**(9-10), 423–426 (2008).
28. R. Y. Golovchak, S. A. Kozyukhin, A. Kozdras, O. Shpotyuk, and V. M. Novotortsev, "Physical aging of chalcogenide glasses," Inorg. Mater. **46**(8), 911–913 (2010).
29. A. Kozdras, R. Golovchak, O. Shpotyuk, S. Szymura, A. Saiter, and J.-M. Saiter, "Light-assisted physical aging in chalcogenide glasses: Dependence on the wavelength of incident photons," J. Mater. Res. **26**(18), 2420–2427 (2011).
30. Amorphous Materials, Inc., retrieved May 2018, http://www.amorphousmaterials.com/.
31. K. Tanaka, Y. Kasanuki, and A. Odajima, "Physical properties and photoinduced changes of amorphous Ge-S films," Thin Solid Films **117**(4), 251–260 (1984).
32. A. Ródenas, G. Martin, B. Arezki, N. Psaila, G. Jose, A. Jha, L. Labadie, P. Kern, A. Kar, and R. Thomson, "Three-dimensional mid-infrared photonic circuits in chalcogenide glass," Opt. Lett. **37**(3), 392–394 (2012).
33. P. Khan, H. Jain, and K. V. Adarsh, "Role of Ge:As ratio in controlling the light-induced response of a-$Ge_xAs_{35-x}Se_{65}$ thin films," Sci. Rep. **4**, 4029 (2014).
34. C. M. Schwarz, C. N. Grabill, G. D. Richardson, S. Labh, A. M. Lewis, A. Vyas, B. Gleason, C. Rivero-Baleine, K. A. Richardson, A. Pogrebnyakov, T. S. Mayer, and S. M. Kuebler, "Fabrication and characterization of microstructures created in thermally deposited arsenic trisulfide by multiphoton lithography," J. Micro/Nanolith. MEMS MOEMS **16**(2), 023508 (2017).
35. H. B. Sun, M. Maeda, K. Takada, J. W. M. Chon, M. Gu, and S. Kawata, "Experimental investigation of single voxels for laser nanofabrication via two-photon photopolymerization," Appl. Phys. Lett. **83**(5), 819–821 (2003).

Optical Materials EXPRESS

36. L. Jonušauskas, D. Gailevičius, L. Mikoliūnaitė, D. Sakalauskas, S. Šakirzanovas, S. Juodkazis, and M. Malinauskas, "Optically clear and resilient free-form μ-optics 3D-printed via ultrafast laser lithography," Materials (Basel) **10**(1), 12 (2017).
37. Y. Kumaresan, A. Rammohan, P. K. Dwivedi, and A. Sharma, "Large area IR microlens arrays of chalcogenide glass photoresists by grayscale maskless lithography," ACS Appl. Mater. Interfaces **5**(15), 7094–7100 (2013).
38. M. Manevich, M. Klebanov, V. Lyubin, J. Varshal, J. Border, and N. Eisenberg, "Gap micro-lithography for chalcogenide micro-lens array fabrication," Chalcogenide Lett. **5**, 61–64 (2008).
39. R. Naik, S. Jena, R. Ganesan, and N. K. Sahoo, "Photo-induced optical bleaching in $Ge_{12}Sb_{25}S_{63}$ amorphous chalcogenide thin films: effect of 532 nm laser illumination," Laser Phys. **25**(3), 1–8 (2015).
40. M. Olivier, P. Nemec, G. Boudebs, R. Boidin, C. Focsa, and V. Nazabal, "Photosensitivity of pulsed laser deposited Ge-Sb-Se thin films," Opt. Mater. Express **5**(4), 781–793 (2015).
41. M. S. Iovu, E. I. Kamitsos, C. P. E. Varsamis, P. Boolchand, and M. Popescu, "Raman spectra of As_xSe_{100-x} and $As_{40}Se_{60}$ glasses doped with metals," Chalcogenide Lett. **2**(3), 21–25 (2005).
42. R. A. Synowicki and T. E. Tiwald, "Optical properties of bulk c-ZrO_2, c-MgO and a-As_2S_3 determined by variable angle spectroscopic ellipsometry," Thin Film Solids **455–456**, 248–255 (2004).
43. J. Hu, V. Tarasov, N. Carlie, L. Petit, A. Agarwal, K. Richardson, and L. Kimerling, "Exploration of waveguide fabrication from thermally evaporated Ge–Sb–S glass films," Opt. Mater. **30**(10), 1560–1566 (2008).
44. S. Noehte, J. Ackermann, K. Schwartz, C. Dietrich, and R. Männer, "Optical grating studies in a-As_2S_3 films using scanning force microscopy," (Universität Mannheim, Mannheim, Germany, 1995).
45. R. J. Weiblen, C. R. Menyuk, L. E. Busse, L. B. Shaw, J. S. Sanghera, and I. D. Aggarwal, "Optimized moth-eye anti-reflective structures for As_2S_3 chalcogenide optical fibers," Opt. Express **24**(10), 10172–10187 (2016).
46. H. E. Williams, "Photophysical and Photochemical Factors Affecting Multi-Photon Direct Laser Writing Using the Cross-Linkable Epoxide SU-8," PhD dissertation (University of Central Florida, Orlando, FL, USA, 2013).
47. V. Kaur, S. K. Tripathi, and S. Prakash, "The electronic structure of As_2S_3," presented at International Conference on Condensed Matter and Applied Physics, Bikaner, Rajasthan, 30 - 31 Oct. 2015.
48. A. Zakery and S. R. Elliot, *Optical Nonlinearities in Chalcogenide Glasses and their Applications Springer Series in Optical Science* (Springer, 2007), Vol. 135.
49. A. Zoubir, M. Richardson, C. Rivero, A. Schulte, C. Lopez, K. Richardson, N. Hô, and R. Vallée, "Direct femtosecond laser writing of waveguides in As_2S_3 thin films," Opt. Lett. **29**(7), 748–750 (2004).
50. D. C. Ghosh and R. Biswas, "Theoretical calculation of absolute radii of atoms and ions. Part 1. The atomic radii," Int. J. Mol. Sci. **3**(2), 87–113 (2002).
51. M. Olivier, J. C. Tchahame, P. Nemec, M. Chauvet, V. Besse, C. Cassagne, G. Boudebs, G. Renversez, R. Boidin, E. Baudet, and N. Nazabal, "Structure, nonlinear properties, and photosensitivity of $(GeSe_2)_{100-x}(Sb_2Se_3)_x$ glasses," Opt. Mater. Express **4**(3), 525–540 (2014).
52. J. E. Huheey, *Inorganic Chemistry: Principles of Structure and Reactivity,* 3rd ed. (Harper and Rowe, New York, 1983).
53. P. Němec, S. Zhang, V. Nazabal, K. Fedus, G. Boudebs, A. Moreac, M. Cathelinaud, and X.-H. Zhang, "Photo-stability of pulsed laser deposited $Ge_xAs_ySe_{100-x-y}$ amorphous thin films," Opt. Express **18**(22), 22944–22957 (2010).
54. C. Mack, *Fundamental Principles of Optical Lithography: The Science of Microfabrication* (John Wiley & Sons Ltd., West Sussex, 2007).

1. Introduction

Infrared (IR) optical systems offer capabilities in spectroscopy, imaging, astrophysics, diagnostic medicine, sensing, safety, defense and environmental monitoring that are not achievable using visible (Vis) and near-infrared (NIR) wavelengths [1–4]. Legacy IR optical materials hinder innovation in these areas because they afford no means for controlling optical, thermal, and mechanical properties. Conventional IR optics created from crystalline Ge, Si, and ZnSe are difficult to process, costly, and have fixed optical, mechanical and thermo-optic properties, which are far from optimum for most applications. Typical processing techniques, such as single-point diamond turning, are expensive and produce brittle optics. Less costly alternatives like molding produce bulky/heavy optics with limited optical functionality [5–13].

Semiconducting photo-patternable multi-component glasses known as chalcogenide glasses (ChGs) possess tunable properties that include excellent IR transparency, large index of refraction, photo-sensitivity, modest coefficients of thermal expansion (CTE), thermo-optic coefficient (dn/dT), and unique optical functionality over a range of form factors and environmental conditions [14]. ChGs have applications in photonic waveguides, sensors, acousto-optics, and optics [14–18].

Micro-scale 3D devices have function in optics, imaging, sensing, consumer electronics, micro-electromechanical systems, and medicine [16–18]. Multiphoton lithography (MPL) has

Optical Materials EXPRESS

been used to create functional micro-scale three-dimensional (3D) devices in photopolymers, glasses, and composites [19]. However, there is a lack of viable semiconductor material systems that can be directly photo-patterned. New semiconductor materials systems are needed to create structures with improved electronic, magnetic, thermal, optical, or mechanical function, or the ability to respond to a chemically active environment, as needed for sensing.

The ChG that has been most used for MPL is thermally deposited arsenic trisulfide (As_2S_3) [15–18]. As_2S_3 offers potential for IR applications due to its useful optical bandgap of $E_g = 2.35$ eV ($\lambda \approx 517$ nm), high transparency from 620 nm to 11 μm, and large refractive index of $n = 2.45 - 2.53$ [15–18]. As_2S_3 can be thermally deposited onto substrates as thin photo-sensitive glassy films of molecular clusters consisting of homopolar bonds. Photo-excitation of the thermally deposited film cross-links the material back into a glassy network solid by converting the homopolar bonds to heteropolar bonds. Photo-patterned As_2S_3 films can then be immersed in a polar solvent to selectively dissolve away unexposed material, revealing the targeted structure. MPL in As_2S_3 films has been used to create 3D structures such as woodpile photonic crystals, waveguide, and nanowires [15]. However, As_2S_3 is unstable toward crystallization, and it forms oxides under ambient conditions, which significantly diminishes its usefulness for practical applications [20]. Additionally, As_2S_3 has fixed optical, mechanical, and thermo-optical properties that are poorly suited for IR applications. No other ChG composition has been comprehensively studied for photo-processing by MPL. New photo-processible ChGs for MPL are needed, including better fundamental understanding of the relationship between their composition and processing and the resulting properties and performance, to enable fabrication of high-performance IR optical and photonic devices.

Ge-doped As/Se ChG glasses offer advantages over As_2S_3 glasses. It has been reported that films are more photo-sensitive when they contain As-Se and Ge-Se molecular units [21]. The polarizability and therefore the index of refraction of the thermally deposited films and the laser patterned structures should increase with Ge content [14]. The inclusion of Ge into the material system is expected to improve the mechanical toughness of the thermally deposited films and the laser patterned structures [22]. Replacing S by Se and adding Ge has been shown to increase the stability of As-based bulk ChGs [23–26]. Comparisons of As/S, As/Se, and Ge/Se ChGs show that Se-containing glasses are more stable toward light-induced ageing [27–29]. Consistent with this, the commercial series of AMTIR glasses based on Ge/As/Se are environmentally stable in bulk form [30]. Additionally, studies of thermally deposited $GeSe_2$ show that Ge scavenges oxygen and remains amorphous, which prevents further crystallization [31]. Therefore, incorporating Ge and Se into a thermally deposited ChG should help stabilize the laser-cross-linked material. To date, MPL in Ge/Se-based thermally deposited films has not been reported, and there are only a few reports of photo-exposure and etch processing of bulk Ge/Se-based ChGs [32].

This work reports the first detailed study of MPL in thermally deposited Ge/Se-based films. Fundamental understanding has been obtained for how chemical composition, laser patterning conditions, and etch processing affect the nano-structure morphology, chemical networking, and appearance of the features generated by MPL in Ge/Se-based films. This knowledge should help advance the use of ChGs for manufacturing IR optics with tunable properties and expanded applications.

2. Methods

2.1 Thermal deposition of films

Bulk $Ge_5(As_2Se_3)_{95}$ and $Ge_5(As_3Se_7)_{95}$ material was thermally deposited onto polished silicon wafers. The bulk ChGs were prepared using traditional melt-quench processes described elsewhere [33]. All films were deposited using a Kurt Lesker thermal evaporation chamber. The substrate temperature was not controlled during deposition. The $Ge_5(As_2Se_3)_{95}$ film was deposited at a rate of 55 Å s^{-1} – 75 Å s^{-1}, had a final thickness of 511 nm ± 6.8 nm, and was

Optical Materials EXPRESS

silver in color. The $Ge_5(As_3Se_7)_{95}$ film was deposited at a rate of 55 Å s^{-1} – 65 Å s^{-1}, had a final thickness of 526 nm ± 4.9 nm, and was also silver in color. The film colors were determined by visual inspection. All films were placed in light-tight containers and stored in a desiccator for protection from ambient light and moisture. The films were prepared and handled as reported earlier [16–18, 34].

2.2 Photo-patterning

The methods of laser exposure and film processing have been described previously but are summarized here for completeness [16–18, 34]. A mode-locked femtosecond laser (Coherent-Mira, 800-nm center wavelength, pulse width τ_p = 120 fs, repetition rate f = 76 MHz) was used to photo-pattern the films. An acousto-optic modulator (AOM) was used to electronically control beam power. The laser beam was first guided through a beam expander then into a 100× /1.4 NA oil-immersion objective (Nikon) which focused the beam in to the film. The transverse spatial profile of the beam is approximated as a radially symmetric Gaussian having a $1/e^2$ radius of $\omega_0 \approx 175$ nm, and the minor effects of input beam polarization are neglected [35]. The laser beam was focused along the z-axis of an arbitrary coordinate system defined so that the substrate lies in the xy-plane. The average power $\langle P \rangle$ used to photo-pattern the films was measured at the exit aperture of the objective using an integrating sphere. The corresponding peak irradiance of the focused beam I_p can be estimated using Eq. (1) [36].

$$I_P = \frac{2\langle P \rangle}{f \omega^2 \pi \tau} \tag{1}$$

The film was affixed to a sample stage that was translated at a speed of 50 μm s^{-1} in the x-, y-, and z-axes relative to the laser beam to define patterns. To produce vertical nano-scale pillars, the film was moved to a given (x, y) coordinate, the AOM was activated, and the film was translated in the z-direction to expose over a vertical length of 1 μm – 2 μm. This exposure distance was necessary to bury the beam up to 1 μm into the substrate and to travel completely through the film thickness.

Sets of nano-pillars referred to as “dose arrays” were photo-patterned over a range of travel speeds and average (avg.) focused laser power that varied from 0.02 mW (1.15 GW cm^{-2}) to 3.0 mW (173 GW cm^{-2}). Individual arrays consisted of a 9 × 9 grid of nano-pillars separated by a pitch of 500 nm. Each array had a starting area of approximately 4 μm × 4 μm which increased based on dose and was separated from the next array by 5 μm. The term “dose array” will hereafter refer to the entire set of 9 × 9 grids of nano-pillars separated by a pitch of 500 nm and fabricated using laser powers that varied from 0.02 mW (1.15 GW cm^{-2}) to 3.0 mW (173 GW cm^{-2}) [34].

2.3 Etch processing

Etch processing conditions were identified that could be used to dissolve unexposed regions of a ChG film selectively, leaving behind material that had been exposed and structurally modified. The optimal etchant would yield structures with excellent contrast (ratio of rates at which the exposed and unexposed material from the same film type dissolve in the etchant) and feature fidelity limited only by the dimensions of the focused laser spot.

Etch studies were performed by immersing as-deposited films in either butylamine, propylamine, neat ethanolamine or solutions of ethanolamine in DMSO. The etching was monitored and recorded visually using a video camera. The recordings were reviewed afterward to obtain measures of the time required to etch the material fully. Propylamine, butylamine and ethanolamine were chosen because they have been reported to be good negative etchants for thermally deposited As_2Se_3 films [21, 37, 38]. Due to the reflectivity of the film layer and the silicon substrate are significantly different, the time at which the etchant reached the film/Si

Optical Materials EXPRESS

interface was easily identifiable from changes in the image contrast. The etch rate is defined per Eq. (2) as the ratio of its thickness to the time required to etch it.

$$\text{Etch Rate} = \frac{\text{Film Thickness}}{\text{Etch Duration}} \tag{2}$$

Photo-patterned films were etched using ethanolamine to reveal the targeted nano-structures. The photo-patterned film was immersed in the etchant for up to 120 minutes and then rinsed in a fresh solution for 15 seconds then immersed in IPA for 2 minutes. Scanning electron microscope (SEM) images of the resulting nano-structures were recorded using a Zeiss ULTRA-55 FEG SEM in top-down and profile views. These images were used to measure the dimensions (*x*- and *y*-widths) and shapes of the features and correlate them with film composition, processing conditions, and fabrication laser power. The *x*- and *y*-widths are not expected to be exactly the same because a linearly polarized beam focused under a high numerical aperture does not produce a rotationally symmetric point spread function [17, 18, 39]. This effect is expected to cause the widths to differ by no more than 10%. Rekstyte et al. reported that the observed elongation of polymerized features due to the polarization of the incident laser beam was attributed to heat diffusion and local overheating and was found to be more pronounced for higher pulse energies, longer wavelengths, and longer pulses [40].

2.4 Spectroscopic and optical characterization

Using micro-Raman spectroscopy the film structure and chemical bonding were explored in as-deposited films or in UV-exposed films. A Bruker Senterra micro-Raman system with an average power of 10 mW and an excitation wavelength of 785 nm was used. The beam was focused using a 10× microscope objective (*NA* = 0.3, *WD* = 15 mm). The focused beam had a diameter of 50 μm – 200 μm. Peaks in the Raman spectra of the films were assigned to the molecular fragment as described in references [14, 33, 41]. As-deposited pristine films were exposed by irradiating samples for two minutes in a Zeta Loctite UV flood chamber equipped with high-pressure mercury lamps that emit broadband UV radiation (65 mW cm^{-2}). An energy-dispersive X-ray spectrometer (EDS, Noran System 7) installed on the SEM was used for elemental analysis of the as-deposited films.

The dispersion of the refractive index of pristine and UV-exposed films was determined using a variable-angle spectroscopic ellipsometer (Woollam M2000). The probe wavelengths ranged from 600 nm to 1600 nm. Focusing optics were used to collect data from regions as small as 100 μm × 100 μm with a spectral resolution of 3 nm at visible wavelengths and 6 nm in the near infrared. A Tauc-Lorentz oscillator method was used to extract the *n* and *k* values [42]. The surface roughness and optical bandgap were allowed to vary as free parameters. Film surface roughness was obtained using a Zygo New View 6300 white light interferometer with a 10× objective. The reported surface roughness is the average of the root mean square (RMS) roughness measured from five 0.70 mm × 0.53 mm sample regions.

3. Results and analysis

3.1 Composition and etch processing

Thermal deposition produced Ge-doped AsSe films that are stoichiometrically similar to their bulk starting materials, compositionally homogeneous, and structurally uniform. SEM images and interferometry measurements showed that the Ge-doped AsSe film surface is smooth and homogenous with an average RMS roughness value of 0.060 μm ± 0.004 μm (Fig. 1). The RMS roughness values for the Ge-doped AsSe film similar to reported RMS roughness values for Ge and Se films in which waveguides have been fabricated [43, 44].

Measurements from energy dispersive X-ray spectroscopy (EDX) of bulk glass and thermally deposited films are shown in Table 1. For the bulk glass, the Ge content was kept low (~5%) because high valence (Ge = 4) tends to favor extended 3D network structures,

Optical Materials EXPRESS

whereas lower valence (As = 3 and S/Se = 2) tends to favor sheet-like and chain structures that promote glass formation [23]. The As-to-Se atomic ratios indicate that thermal deposition produced samples similar to the expected stoichiometric elemental composition; however, the Ge content was lower than expected for both films.

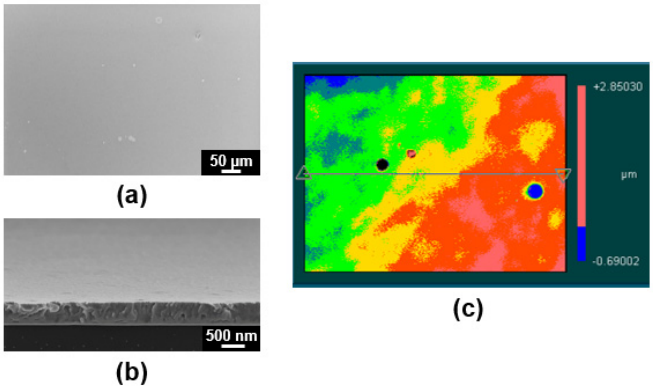

Fig. 1. (**a**) Top-view and (**b**) profile SEM image of a pristine $Ge_5(As_2Se_3)_{95}$ film. (**c**) Example of a surface profile interferogram (area = 0.371 mm^2) obtained for a $Ge_5(As_2Se_3)_{95}$ using white-light interferometry. The circles are small voids which are most likely a result of non-optimized deposition conditions.

Ethanolamine dissolved the as-deposited $Ge_5(As_2Se_3)_{95}$ in 60 minutes, whereas etching in propylamine and butylamine required over 120 minutes and left behind material on the surface. The variation in dissolution kinetics among the amines is likely due to the difference in each solvents polarity [37]. Ethanolamine has the highest polarity out of the three and dissolved the as-deposited film faster and more completely than propylamine or butylamine [37]. Ethanolamine, even with its relatively low rate compared to As_2S_3 (0.139 nm s^{-1} ± 0.02 nm s^{-1} compared to an average value of 18.8 nm s^{-1} ± 6 nm s^{-1} for As_2S_3 films) was the fastest etchant amongst the amines and therefore used as the developer for all further experiments with $Ge_5(As_2Se_3)_{95}$ film. The as-deposited $Ge_5(As_3Se_7)_{95}$ film remained unchanged after immersing in either ethanolamine, propylamine, or butylamine for over 120 minutes.

Table 1. EDX measurements of $Ge_5(As_2Se_3)_{95}$ film and comparison to bulk glass used for thermal deposition.

$Ge_5(As_2Se_3)_{95}$	As Atomic %	Se Atomic %	Ge Atomic %
Bulk	36.76 ± 3.55	56.75 ± 3.46	5.10 ± 0.64
Deposited film	41.15 ± 3.45	56.84 ± 4.62	2.03 ± 0.87

UV exposed $Ge_5(As_2Se_3)_{95}$ films did not show any signs of dissolution after being immersed in ethanolamine for over 120 minutes. UV exposed $Ge_5(As_2Se_3)_{95}$ films also have a slightly higher content of heteropolar bonds. Kumaresan et al. reported that UV exposed As_2Se_3 films have an increased fraction of As-Se heterpolar bonds over as-deposited films and that these heterpolar bonds are responsible for slower etching [37]. This is consistent with the as-deposited $Ge_5(As_3Se_7)_{95}$ film, which has a higher Se content, resisting etching completely.

3.2 Photo-patterning in $Ge_5(As_2Se_3)_{95}$

Dose arrays like those shown in Fig. 2 were used to study the exposure conditions needed to photo-pattern the films. $Ge_5(As_2Se_3)_{95}$ and $Ge_5(As_3Se_7)_{95}$ films were exposed over a range of average focused laser powers (corresponding peak irradiance can be found in Fig. 3) at a fixed scan speed to identify the minimum power needed to create robust features which could survive

Optical Materials EXPRESS

photo-exposure and subsequent etching. Also measured was the maximum power above which damage or distortion occurs, and how the feature size scales with power between the lower and upper limits. After exposure, the unexposed films were removed by etching with ethanolamine.

The $Ge_5(As_3Se_7)_{95}$ films could not be photo-patterned, only ablated (not shown). The apparent ablation threshold is at 1.1 mW. The difference in photo-sensitivity of the two films is due to differences in Se content and resulting As-Se bonds. Additionally, the complete resistance to amine-based etchants would make it impossible to etch away unexposed material and reveal the photo-patterned structures. Given that no viable nano-structures were formed as a result of laser exposure in $Ge_5(As_3Se_7)_{95}$ films, and the film could not be etched, the rest of the photo-patterning and characterization studies were conducted only using $Ge_5(As_2Se_3)_{95}$ films.

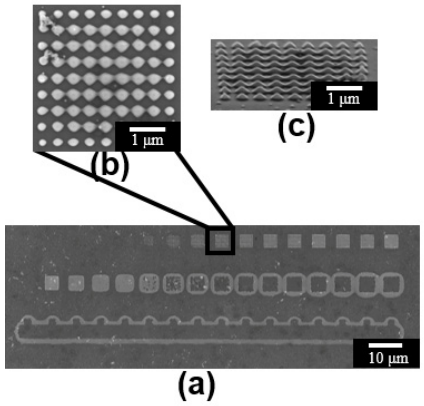

Fig. 2. (**a**) Top-view of a dose array patterned in a $Ge_5(As_2Se_3)_{95}$ film at average powers ranging from 0.050 mW – 2.7 mW (*bottom row*) and 0.020 mW – 0.20 mW (*top row*). The fiduciary marker sits just below each individual array with small marks indicating its location. (**b**) Expanded top-view of an array patterned at 0.10 mW. (**c**) Expanded profile view of the array patterned at 0.10 mW.

Vertically scanning the focal spot through the films during MPL was expected to produce cylindrical pillars, or possibly bead shaped pillars, based on other studies using As_2S_3 films [16]. However, micro-structures patterned in the $Ge_5(As_2Se_3)_{95}$ film are pyramid shaped and smaller (~250 nm) than the film height (~500 nm). The form of the micro-structure suggests a differential etching rate which may be due to cross-linking at the substrate during thermal deposition on an uncooled sample stage. A stronger amine based etchant must be used for $Ge_5(As_2Se_3)_{95}$ films since it is more resistant to amine-based etchants than As_2S_3 films [37]. The increased etchant strength along with the low etch rate of the film suggest that some of the photo-patterned material is also unintentionally etched. This decrease in etch selectivity may cause structure deformation and height decrease. Even though the fabrication did not result in the production of cylindrical or bead shaped nano-structures, the pyramid shaped nano-structures may be useful for creating graded index AR coatings [45].

Exposing the films with higher average laser power produced larger features in the $Ge_5(As_2Se_3)_{95}$ film, consistent with that typically found for a threshold-dependent photochemical process [34, 46]. SEM top-view images were used to obtain the widths of the photo-patterned micro-structures over a range of powers. The measurements were used to create a plot of pillar widths versus power (Fig. 3). For a threshold-dependent MPL process, the relationship between laser-patterned structure-width, spot size of the focused laser beam r_0, average laser power $\langle P \rangle$, and the threshold laser power for producing a feature $\langle P \rangle_{Th}$ can be described by Eq. (3) [46].

Optical Materials EXPRESS

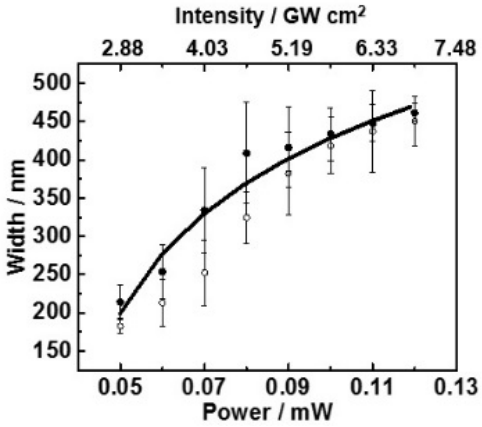

Fig. 3. Widths of nano-fabricated features measured in the *x*- (*open circles*) and *y*-direction (*filled circles*) versus average laser power and peak irradiance for structures patterned in the $Ge_5(As_2Se_3)_{95}$ film.

In Fig. 3, the smooth curve is a global fit of the pillar widths to Eq. (3) with r_0 and $\langle P \rangle_{Th}$ set as free parameters. The fit is consistent with photo-patterning in $Ge_5(As_2Se_3)_{95}$ resulting from a threshold-dependent process. However, deviations from the theoretical curve may be due to variations in the widths of features measured over a given array. Due to the pyramid shape nature of the micro-structures, accurate measurements of the structure width are difficult to obtain. Furthermore, the structure widths may vary across an array as the high viscosity of the etchant increases the potential for uneven etching of the material.

$$\text{Feature-width} = r_o \sqrt{2 \ln \frac{\langle P \rangle}{\langle P \rangle_{Th}}} \tag{3}$$

The $Ge_5(As_2Se_3)_{95}$ films were found to be more photo-sensitive than thermally deposited As_2S_3 [16–18]. Structures with widths of 200 nm are formed at an average power of 0.050 mW. In comparison, an average power of 0.18 mW is needed to produce this sized feature in As_2S_3 films. The apparent increased photo-sensitivity of thermally deposited $Ge_5(As_2Se_3)_{95}$ results from the addition of Se and Ge into the system. The electronic band gap for bulk As_2S_3 and As_2Se_3 is 1.93 eV and 1.1 eV, respectively [47, 48]. The electronic band-edge of bulk $As_2S_{1-x}Se_x$ red-shifts with increasing Se content. If the same can be expected for thermally deposited films, then increasing the Se-content should produce a more photo-sensitive ChG film at a given wavelength. Thermal deposition of As_2S_3 is known to produce films containing molecular clusters with homopolar As-As and S-S bonds that allow facile bond cleavage and network cross-linking with photo-excitation [16–18, 49]. Ge atoms are more polarizable than S atoms [50], and the electronic band-edge of bulk ChGs also red-shifts with increasing Ge content [51]. Consequently, increasing the Ge content of thermally deposited films should also increase their linear and nonlinear absorptivity [23,51] making them more photo-sensitive. The photo-sensitivity of a material also depends on the strength of bonds being activated with light. Materials having weaker bonds will be more photo-sensitive at a given wavelength. The photo-sensitivity of thermally deposited chalcogenide glasses originates with the homopolar bonds. The bond dissociation energies for S-S and Se-Se bonds are 226 kJ/mol and 172 kJ/mol, respectively [52]. Given that Se-Se bonds are weaker than S-S bonds, and As/Se glasses are more absorptive than As/S glasses at the same wavelength, AsSe glasses can be expected to be more photo-sensitive.

Optical Materials EXPRESS

3.3 Raman spectroscopy of $Ge_5(As_2Se_3)_{95}$ films

Raman spectroscopy was used to study the chemical structure of bulk-, as-deposited-, and UV-exposed films (*circa* 1 μm Raman sampling depth). In Fig. 4, Raman spectra of the film have peaks indicative of molecular clusters typically found in thermally deposited films containing Ge, As, and Se [21]. The peak appearing at 300 cm^{-1} is due to the silicon substrate. The film displays low-energy peaks at 203 cm^{-1}, 215 cm^{-1}, 223 cm^{-1}, 238 cm^{-1}, 240 cm^{-1}, 248 cm^{-1} indicating the presence of Ge_2Se_4, $GeSe_4$, $AsSe_3$, As_4Se_3, As_2Se_3 and As_4Se_4 molecular clusters, respectively (Table 2) [14, 33, 41, 53]. In Fig. 4, the peak at 256 cm^{-1} is assigned to $AsSe_3$ and the broad shoulder at 265 cm^{-1} is assigned to Se_8 rings. The film lacks the sharp Ge_2Se_4 peak which is found for the bulk glass (Fig. 4). This indicates that thermal deposition rearranges the Ge/Se bonds to form the molecular clusters that transport through the vapor phase to the substrate, just as is observed for thermal deposition of As_2S_3 [34].

Table 2. Assignment of peaks observed by Raman spectroscopy for thermally deposited chalcogenides.

Molecular clusters	Wavenumber / cm^{-1}	Molecular clusters	Wavenumber / cm^{-1}
Ge_2Se_4	203	As_4Se_3	238
$GeSe_4$	215	As_2Se_3	240
$AsSe_3$	223	As_4Se_4	248

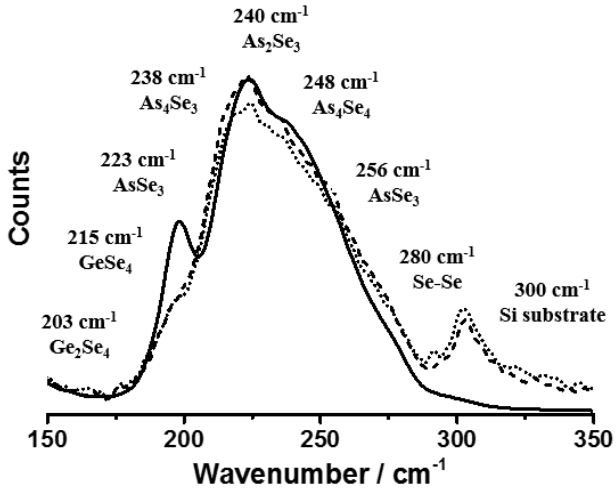

Fig. 4. Raman spectra of $Ge_5(As_2Se_3)_{95}$ in bulk form (*solid line*), as a thermally deposited film (*dashed line*), and as a UV-exposed film (*dotted line*).

Figure 4 also shows how the $Ge_5(As_2Se_3)_{95}$ film behaves under UV-exposure. The bands at 203 cm^{-1}, 215 cm^{-1}, 223 cm^{-1}, 238 cm^{-1}, 240 cm^{-1}, and 248 cm^{-1} decrease slightly following UV exposure, indicating that irradiation breaks or rearranges the homopolar bonds of Ge_2Se_4, $GeSe_4$, $AsSe_3$, As_4Se_3, As_2Se_3 and As_4Se_4 units in the glassy film. These findings are consistent with previous studies of Ge- and Se-based films [21, 38]. Khan et al. reported that the local glass energy increases with the ratio of edge-sharing to corner-sharing Ge_2Se_4 bonds, so laser irradiation of $Ge_xAs_{35-x}Se_{65}$ thin films relaxes the glass-energy by removing the edge-sharing bonds [21]. Similarly, Olivier and associates reported that there was a decrease in homopolar Ge-Ge bonds after irradiation of thermally deposited $(GeSe_2)_{70}(Sb_2Se_3)_{30}$ films [38].

Optical Materials EXPRESS

3.4 Index of refraction for as-deposited films

The index of refraction n and extinction coefficient k were obtained from spectroscopic ellipsometry measurements performed on as-deposited $Ge_5(As_2Se_3)_{95}$ film (Fig. 5). The extinction coefficient k (not shown) was effectively zero for the film over the 500 nm to 1600 nm wavelength range. The index of refraction n of the $Ge_5(As_2Se_3)_{95}$ film is approximately 0.446 units greater than that of thermally deposited As_2S_3 [34]. The high refractive index and photo-sensitivity of the $Ge_5(As_2Se_3)_{95}$ film suggests that thermally deposited Ge/Se-based films could be useful for fabricating functional infrared photonic devices.

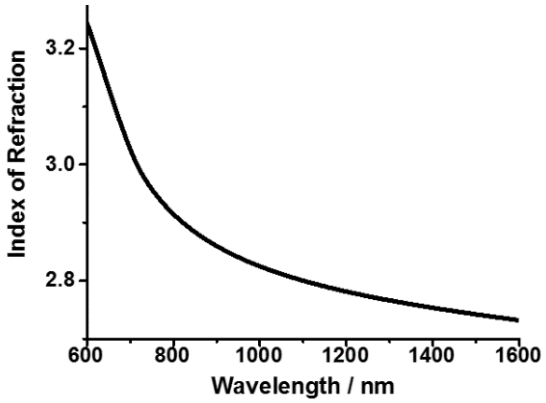

Fig. 5. Optical properties of the pristine $Ge_5(As_2Se_3)_{95}$ film, as measured by ellipsometry. The extinction coefficient κ (not shown) has values at or near zero ($\kappa \leq 0.13$).

3.5 Stability of structures photo-patterned in $Ge_5(As_2Se_3)_{95}$

The stability of structures photo-patterned in $Ge_5(As_2Se_3)_{95}$ was compared to those created using As_2S_3 and correlated with the environmental conditions, age, and composition of the parent-films. The surfaces of thermally deposited As_2S_3 films are known to become chemically altered and degraded due to exposure to ambient light and water vapor [20]. Key attributes of the aged As_2S_3 materials which make them unsuitable for use (without a protective layer that mitigates environmental degradation) is that both homogeneous and patterned films exhibit surface crystallization and thus, increased optical loss with age. Before photo-patterning, as-deposited films were kept in closed petri dishes wrapped with aluminum foil and stored in an amber desiccator in a cupboard to minimize exposure to ambient light and humidity. After a film was photo-patterned and etched, the resulting micro-structures were stored in closed petri dishes in a cupboard, but permitted to have contact with ambient air and humidity. To compare the stability of films and structures produced with $Ge_5(As_2Se_3)_{95}$ and As_2S_3, SEM imaging and EDX spectroscopy were used to monitor the samples over time and detect changes in morphology, film topography, and chemical structure.

SEM images revealed that after three months, micro-structures created in As_2S_3 were significantly degraded (Fig. 6), whereas micro-structures created in $Ge_5(As_2Se_3)_{95}$ were unchanged. Features patterned in As_2S_3 had deformed and excess material formed on the surface of the micro-structures. EDX showed that this degradation included both crystallization and formation of As_2O_3. Un-patterned, as-deposited films of As_2S_3 degraded similarly within three months (Figs. 6g and 6h). It was also found that as As_2S_3 films age, their photo-sensitivity decreases. In contrast, films and micro-structures created in $Ge_5(As_2Se_3)_{95}$ are much more robust. After four years, structures photo-patterned in $Ge_5(As_2Se_3)_{95}$ at low power had shrunk slightly, but as seen in Fig. 7, features patterned at intermediate powers were largely unchanged. Additionally, neither as-deposited films of $Ge_5(As_2Se_3)_{95}$ nor micro-structures created in $Ge_5(As_2Se_3)_{95}$ exhibited any signs of surface crystallization. Raman and EDX spectroscopy of a square pad of laser-patterned and etched $Ge_5(As_2Se_3)_{95}$ that was aged for four years exhibited

Optical Materials EXPRESS

no change in atomic composition or chemical bonding within experimental error (Table 3 and Fig. 8). Thus, adding Ge and Se elements into the composition increases the stability of the films and decreases degradation with time relative to As_2S_3 films. These observations show that ChGs for MPL based on Ge and Se would be more stable than As_2S_3. This conclusion is important, because although more aggressive etchants are needed to process $Ge_5(As_2Se_3)_{95}$, the material is clearly better suited than As_2S_3 for creating nano- and micro-scale devices.

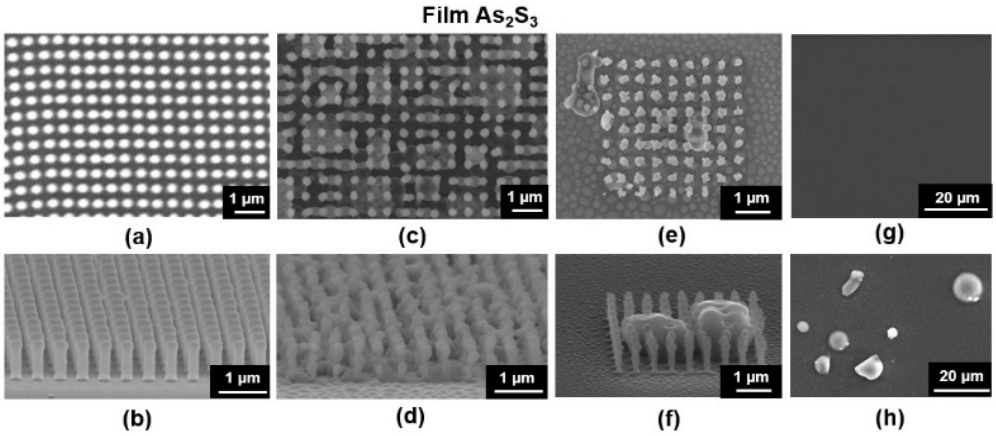

Fig. 6. (**a**) Top-down and (**b**) side-view SEM images of nano-pillars fabricated by MPL in thermally deposited As_2S_3. (**c**) Top-down and (**d**) side-view images of the same structures after storing for three months in the dark and ambient air. (**e**) Top-down As_2S_3 dose array pillar micro-structures after three months showing excess material in array and on substrate surface. (**f**) Side-view As_2S_3 dose array pillar micro-structures after three months showing excess material in array and on substrate surface. (**g**) As-deposited As_2S_3 film. (**h**) As-deposited film after three months showing excess material and crystallization.

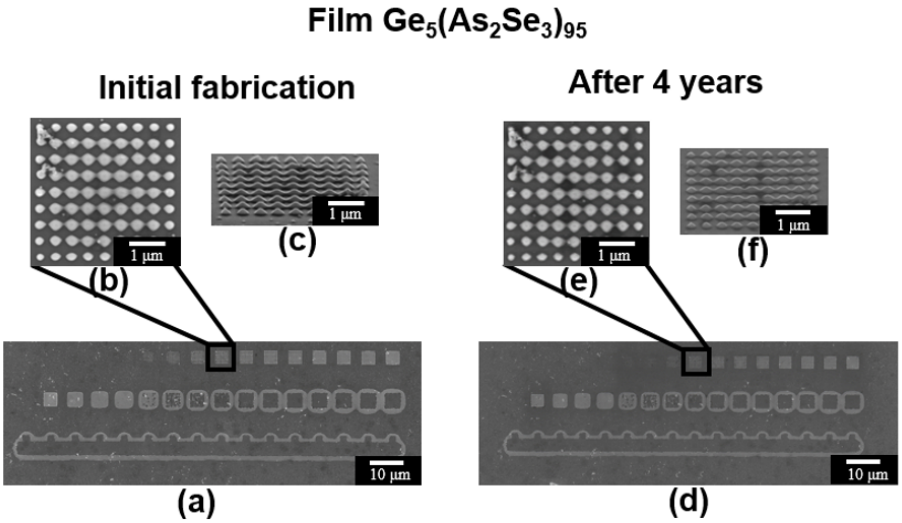

Fig. 7. (a) Top-view of a dose array patterned at average powers ranging from 0.050 mW – 2.7 mW (*bottom row*) and 0.020 mW – 0.20 mW (top row). The fiduciary marker sits just below each individual array with small marks indicating its location. (b) Expanded top-view of an array patterned at 0.10 mW. (c) Expanded profile view of the array patterned at 0.10 mW. (d) Top-view of a dose array patterned at average powers ranging from 0.050 mW – 2.7 mW (*bottom row*) and 0.020 mW – 0.20 mW (*top row*) after four years. (e) Expanded top-view of an array patterned at 0.10 mW after four years. (f) Expanded profile view of the array patterned at 0.10 mW after four years of aging.

Optical Materials EXPRESS

It is important to note that the slow etching rate and low contrast is a disadvantage with Ge/Se containing films as compared to As_2S_3 films. However, some organic resists etch slowly and have low etch selectivity have been used for anti-reflective coatings [54]. Therefore, it is still reasonable that this material can be useful for manufacturing. In future work, thicker films as well as different deposition rates which are known to influence the etch rate of the film will be explored.

Table 3. EDX measurements of $Ge_5(As_2Se_3)_{95}$ film and four year old laser-exposed pad.

$Ge_5(As_2Se_3)_{95}$	As Atomic %	Se Atomic %	Ge Atomic %
As-deposited film	41.15 ± 3.45	56.84 ± 4.62	2.03 ± 0.87
Aged, laser-exposed pad	45.43 ± 4.02	51.53 ± 4.32	3.03 ± 1.59

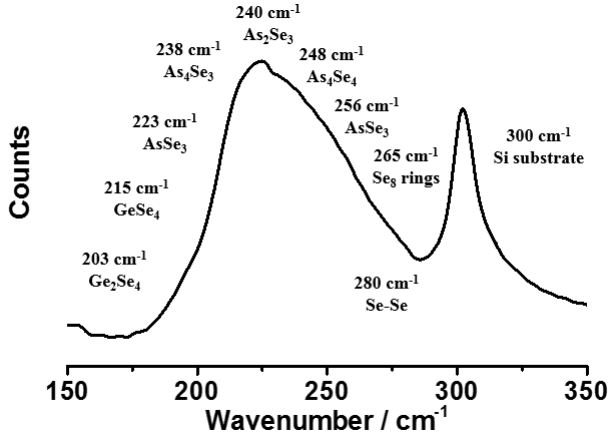

Fig. 8. Raman spectrum of a pad of laser-patterned and etched $Ge_5(As_2Se_3)_{95}$ after four years of aging. The band due to the substrate (300 cm^{-1}) appears stronger relative to that seen in Fig. 4 because etching after laser-exposed removes some $Ge_5(As_2Se_3)_{95}$.

4. Conclusions

Compositions based on Ge-doped arsenic selenide were investigated to find new materials for MPL that offer higher stability as thermally deposited films and patterned structures than As_2S_3. Thermal deposition of $Ge_5(As_2Se_3)_{95}$ formed glassy films that were more photo-sensitive than As_2S_3, enabling fabrication at lower average power. Nano-structures created in $Ge_5(As_2Se_3)_{95}$ had a pyramid shape, which may be useful for a creating graded index anti-reflective surfaces. The addition of Ge and Se stabilizes the chalcogenide glass and decreases the degradation effects typical of As_2S_3. The increased photo-sensitivity, higher index, and improved stability of $Ge_5(As_2Se_3)_{95}$ suggests that Ge/Se-based chalcogenides may better suited for manufacturing via MPL of functional optical and photonic devices with improved optical, mechanical, and thermal properties.

Funding

National Science Foundation (NSF CAREER award DMR/CHE-0748712 and DMR-1337758); Lockheed Martin; the Florida High-Tech Corridor Council; the Space Research Initiative Program, through the Florida Space Institute, hosted at the University of Central Florida; and the National Aeronautics and Space Administration, through the University of Central Florida's NASA-Florida Space Grant Consortium.

Optical Materials EXPRESS

Acknowledgments

The authors thank Dr. Pieter Kik and Dr. Chatdanai Lumdee for assistance with the ellipsometry measurements and Dr. Claudia Goncalves for additional Raman measurements. GDR and SL were supported by UCF SURF scholarships.